Review of Scientific Instruments

Fast ion energy distribution from third harmonic radio frequency heating measured with a single crystal diamond detector at the Joint European Torus

Cite as: Rev. Sci. Instrum. **86**, 103501 (2015); https://doi.org/10.1063/1.4931755
Submitted: 21 June 2015 . Accepted: 10 September 2015 . Published Online: 01 October 2015

M. Nocente, C. Cazzaniga, M. Tardocchi, F. Binda, J. Eriksson, L. Giacomelli, A. Muraro, M. Rebai, S. Sharapov, G. Gorini, and JET Contributors

Fast ion energy distribution from third harmonic radio frequency heating measured with a single crystal diamond detector at the Joint European Torus

M. Nocente,[1,2,3] C. Cazzaniga,[1,3,4] M. Tardocchi,[1,3] F. Binda,[1,5] J. Eriksson,[1,5] L. Giacomelli,[1,3] A. Muraro,[1,3] M. Rebai,[1,2,3] S. Sharapov,[1,6] G. Gorini,[1,2,3] and JET Contributors[1,a)]

[1]*EUROfusion Consortium, JET, Culham Science Centre, Abingdon, OX14 3DB, United Kingdom*
[2]*Dipartimento di Fisica "G. Occhialini," Università degli Studi di Milano-Bicocca, Milano, Italy*
[3]*Istituto di Fisica del Plasma "P. Caldirola," Consiglio Nazionale delle Ricerche, Milano, Italy*
[4]*Rutherford Appleton Laboratory, ISIS Facility, Didcot, United Kingdom*
[5]*Department of Physics and Astronomy, Uppsala University, Uppsala, Sweden*
[6]*CCFE, Culham Science Centre, Abingdon, Oxfordshire OX14 3DB, United Kingdom*

(Received 21 June 2015; accepted 10 September 2015; published online 1 October 2015)

Neutron spectroscopy measurements with a single crystal diamond detector have been carried out at JET, for the first time in an experiment aimed at accelerating deuterons to MeV energies with radio frequency heating at the third harmonic. Data are interpreted by means of the expected response function of the detector and are used to extract parameters of the highly non-Maxwellian distribution function generated in this scenario. A comparison with observations using a time of flight and liquid scintillator neutron spectrometers is also presented. The results demonstrate the capability of diamond detectors to contribute to fast ion physics studies at JET and are of more general relevance in view of the application of such detectors for spectroscopy measurements in the neutron camera of next step tokamak devices. [http://dx.doi.org/10.1063/1.4931755]

I. INTRODUCTION

Neutron spectroscopy measurements are of paramount importance for high power fusion plasmas diagnostics. They can be used to extract essential parameters for machine control, such as the fuel ion temperature,[1] the thermal/non-thermal components of the neutron emission,[2,3] and the fuel ion ratio.[4] More recently, they have contributed to fundamental studies on the physics of suprathermal ions in thermonuclear plasmas, mostly by detailed measurements of the distribution function of the energetic ions[5–7] and their effects on the plasma stability.[8,9]

Advanced neutron spectroscopy measurements are nowadays performed along a single, collimated line of sight by means of dedicated, non-compact detectors, based on the time of flight technique[10–12] for deuterium-deuterium (dd) fusion neutrons and on proton recoil for deuterium-tritium (dt).[13] These instruments typically show a good energy resolution (between 5% and 7%) and a wide dynamic range sensitivity (up to 5 orders of magnitude in the case of proton recoil) that allows detecting even the very small components (at the 10^{-3}–10^{-5} level) induced by fast ion nuclear elastic scattering in the plasma.[14–16]

Besides detailed spectroscopy measurements at high accuracy along a single line of sight, there is, however, a need to enable spectroscopic information in measurements along multiple collimated lines of sight (e.g., in a neutron camera system), where the use of present days, non-compact spectrometers is impeded by practical considerations. A possibility is offered by recent advances in the production of chemical vapor deposition, single crystal diamond detectors (SDDs) that, being compact, radiation resistant, and insensitive to magnetic fields, are ideal candidates for this type of application.[17–19] Prior to SDDs, natural diamond detectors were used for neutron flux and spectroscopy measurements in selected discharges of the dt campaigns at TFTR[20] and JET.[21] These pioneering measurements demonstrated the use of diamond detectors as compact neutron spectrometers for fusion plasma applications, but suffered from a rather limited statistics due to the low detection efficiency of natural diamonds. This, combined with the high cost and little reproducibility of the devices, discontinued the use of such detectors for neutron spectroscopy applications. The recent availability of SDDs with superior electrical properties than natural diamonds, combined with an excellent reproducibility at a significantly reduced cost, has renewed the interest in diamond based detectors for neutron spectroscopy applications. Compared to other more conventional types of compact detectors, such as 1 in. × 1 in. liquid scintillators (or NE213), SDDs with typical commercial dimensions (a few mm^2) have a reduced detection efficiency by a factor ≈100, which make them not particularly suited for applications at low neutron fluxes (say $<10^5$ cm^{-2} s^{-1}). On other hand, the natural role of SDDs is to complement liquid scintillators for measurements at higher neutron fluxes, when excessive pileup and stability issues associated to operations of NE213 detectors at high counting rates may limit their applicability, besides the already mentioned immunity of SDDs to magnetic fields.

In this paper, we report on neutron spectroscopy measurements with a SDD carried out at in a recent deuterium experiment at JET (summer 2014), for the first time in a plasma

a)See the Appendix of F. Romanelli *et al*. Proceedings of the 25th IAEA Fusion Energy Conference 2014, Saint Petersburg, Russia.

with 3rd harmonic ion cyclotron resonance heating (ICRH) coupled into an injected deuterium beam.[23] This scenario, which is particularly effective at accelerating deuterium ions to the MeV range as previously demonstrated,[5,24,25] is of relevance for fast ion physics studies in a deuterium plasma. Here, we show, in particular, that SDD data can be used to extract parameters of the highly non-Maxwellian fast ion energy distribution generated in the experiment by detailed modeling of the instrument response function and the emission spectrum of the fusion neutrons born in the plasma. Parameters of the fast ion energy distribution derived from SDD data are compared to observations with other neutron spectrometers at JET, such as the Time Of Flight Optimised for Rate (TOFOR) instrument and a NE213 liquid scintillator detector,[26] and their sensitivity to measured data is discussed.

II. INSTRUMENTATION AND RESPONSE FUNCTION

The single crystal diamond detector used for these measurements has an active volume of 4.7×4.7 mm^2 $\times$ 0.5 mm (thickness) with circular aluminum contact (4.5 mm diameter) and was first installed at JET in 2013.[27] The detector is housed in the beam dump of the Magnetic Proton Recoil Upgrade (MPRu) neutron spectrometer[13] and shares its same line of sight, viewing the plasma along a collimated cone with an angle of about 47° with respect to the magnetic field at the plasma center. Under normal operations, a bias voltage of +400 V is applied to the detector contacts. The readout chain consists of a fast CIVIDEC C6[28] pre-amplifier that is placed about 20 cm away from the SDD (out of the incoming neutron beam) and is the first amplification stage, meant for 14 MeV neutron measurements. A second amplification stage is needed for DD neutron measurements due to the smaller energy deposited by these neutrons in the device and is obtained by means of a 20 dB CIVIDEC C1 current pre-amplifier[28] in cascade to the C6. Amplified signals from the Torus Hall are then propagated along a 120 m BNC cable connecting the detector to the data acquisition in the JET Diagnostic Hall. Here, signals are digitized by means of a CAEN DT5751 waveform digitizer (four channel, 1 GHz, 10 bit, input range: 0–1 V) and stored on a local computer. Analysis of the recorded waveforms is done offline, typically after each discharge of interest. The energy calibration is provided by a triple-α source (^{241}Am, ^{239}Pu, and ^{244}Cm) that is available close to the detector and gives a reference signal at a counting rate <10 Hz. The signal full width at half maximum (FWHM) from the α source is about 20 ns after the long BNC cable (compared to ≈10 ns before the cable), which guarantees an acceptable signal pileup probability even at counting rates approaching 1 MHz, as expected in high power DT operations at JET. The energy resolution measured at 5.2 MeV is 2.2% and extrapolates to 8% for 2.5 MeV neutrons. Further details on the instrumental setup can be found in Ref. 27.

Diagnostic information is extracted from measurements by comparing data with the expected energy deposition spectrum by interactions between the impinging neutron field and the SDD. This is evaluated discharge by discharge based on a model for the distribution function of the plasma fuel ions (see below). Knowledge of the instrument response function

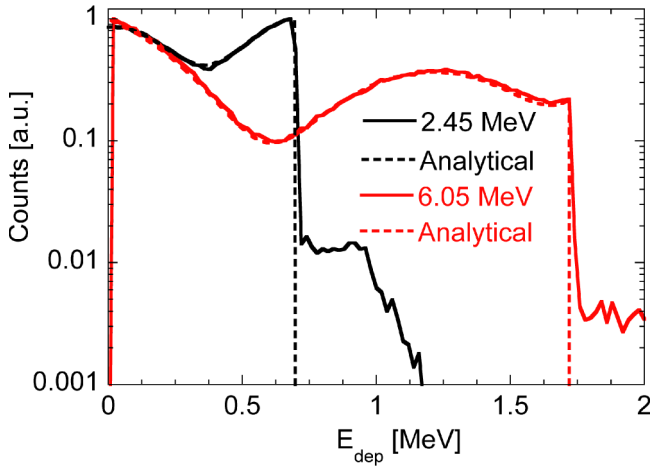

FIG. 1. Calculated response function of the diamond detector installed at JET at impinging neutron energies of 2.45 (black) and 6.05 MeV (red). The solid curves are results obtained with the MCNP code. Results from an analytical calculation in case of single neutron scattering in the device are also shown at each energy for comparison (dashed lines). E_{dep} is the deposited energy.

at each energy of the incoming neutrons (E_n) is needed to evaluate their interaction with the device. To this end, the MCNP code[29] was used to calculate the response matrix of the detector for neutron energies E_n up to 8 MeV, every 0.01 MeV. Examples for a few representative cases are shown in Figure 1. The dominant neutron interaction mechanism with the SDD is nuclear elastic scattering on ^{12}C nuclei in the detector. This gives a characteristic box-like shape to the response function (see Figure 1), with an end point at a deposited energy $E_{dep} = 0.284 \times E_n$ and a modulation reflecting anisotropies in the differential cross sections for n+^{12}C scattering. A comparison between the MCNP results and an analytical calculation in case of a single scattering event in the device at E_n = 2.45 MeV (Figure 1) reveals that the latter is dominant. The analytical calculation is based on the relation between the scattering angle in the c.m. frame $\theta_{c.m.}$ and E_{dep}, i.e.,[22]

$$E_{dep} = \frac{2A}{(1+A)^2}(1 - \cos\theta_{c.m.}) \cdot E_n, \qquad (1)$$

where A = 12. This implies that the number of recoil ^{12}C nuclei generated by a neutron impinging on the device is simply proportional to the differential cross section $\frac{d\sigma}{d\Omega}(\cos\theta_{c.m.})$ of the elastic n+^{12}C scattering where, for a given E_n, $\cos\theta_{c.m.}$ depends on E_{dep} through Eq. (1). Thus, the shape of the response function due to single elastic scattering essentially reflects the angular dependence of $\frac{d\sigma}{d\Omega}(\cos\theta_{c.m.})$. Multi-scattering occurs at the 1% level only and is mostly manifested as a tail of events extending beyond the end point at E_{dep} = 0.7 MeV.

For neutron energies exceeding 4.81 MeV, a new interaction channel opens up as incoming neutrons can diffuse by inelastic collisions on ^{12}C nuclei, leaving the latter in their first excited state at 4.44 MeV. This interaction, which is typically not important to understand data from a deuterium plasma heated by neutral beam injection (NBI) only, must be accounted for in the case of third harmonic ICRH, where the reactant ions can be accelerated to few MeVs.[5,23,24] The

resulting signature in the response function is illustrated, together with multi-scattering, by the difference between the solid and dashed curves of Figure 1 at $E_n = 6.05$ MeV. Similarly to the $E_n = 2.45$ MeV case, inelastic scattering gives little contributions to the response function and is seen as an enhancement at the percent level of events at low ($E_{dep} < 0.5$ MeV) and high ($E_{dep} > 1$ MeV) deposited energies.

III. FAST ION ENERGY DISTRIBUTION FROM 3RD HARMONIC RADIO FREQUENCY (RF) HEATING

The fast ion energy distribution obtained by coupling ICRH at the third harmonic to an injected deuteron beam is highly non-Maxwellian and can be approximated by a one dimensional, semi-analytical model that follows from a generalization of the Stix formalism to heating at multiple harmonics.[30] In a former investigation,[31] this model was found to describe well full results of PION modelling of the distribution function for hydrogen ICRH at the 2nd harmonic and was further validated against neutron spectroscopy measurements in a previous JET experiment based on deuteron ICRH at the third harmonic (see Ref. 5). Therefore, it is also adopted as a reference model for this work.

Since ICRH waves mostly transfer energy to the perpendicular particle motion, we can assume the perpendicular component of the ion velocity vector $v_\perp$ to significantly exceed the parallel one ($v_\parallel$), so that the energy distribution of the fast ions driven to the MeV range by radio frequency is described by $v_\perp$ only and is the solution of the steady-state Fokker-Planck equation

$$0 = \frac{\partial f}{\partial t} = \frac{1}{v_\perp}\frac{\partial}{\partial v_\perp}\left[-\alpha v_\perp f + \frac{1}{2}\frac{\partial}{\partial v_\perp}(\beta v_\perp f) + \frac{1}{4}\gamma f + D_{\mathrm{RF}} v_\perp \frac{\partial f}{\partial v_\perp}\right] + S(v_\perp) + L(v_\perp). \quad (2)$$

Here, α, β, and γ are the Coulomb diffusion coefficients as given by Spitzer[30] and D_{RF} is the quasilinear RF diffusion coefficient, described by

$$D_{RF} = C_{RF}\left|J_{n-1}\left(\frac{k_\perp v_\perp}{\omega_{\mathrm{ci}}}\right) + \frac{E_-}{E_+}J_{n+1}\left(\frac{k_\perp v_\perp}{\omega_{\mathrm{ci}}}\right)\right|^2, \quad (3)$$

where $k_\perp$ is the perpendicular wave number of the RF wave field and ω_{ci} is the cyclotron frequency of the resonating ions. C_{RF} is a constant proportional to the absorbed RF power per particle and $E_\pm$ denotes the left handed (+) and right handed (−) component of the electric field at the resonance. The index $n = 1, 2, 3, \ldots$ is the harmonic number of the heating; $n = 3$ for the case under study in this paper. Measured bulk plasma parameters can be used together with cold-plasma wave theory equations[24,30] to calculate all of the unknown quantities appearing in Eqs. (2) and (3), except for $k_\perp$ and C_{RF}, which are here regarded as free parameters of the model to be derived from measured SDD data.

An example of distribution function calculated by solving Eq. (2) with typical JET parameters is shown in the top part of Figure 2, with the corresponding quasilinear diffusion coefficient displayed in the bottom. $k_\perp$ and C_{RF} were set to 47.5 m^{-1} and 9×10^{13} m^2 s^{-3}, respectively, which were found

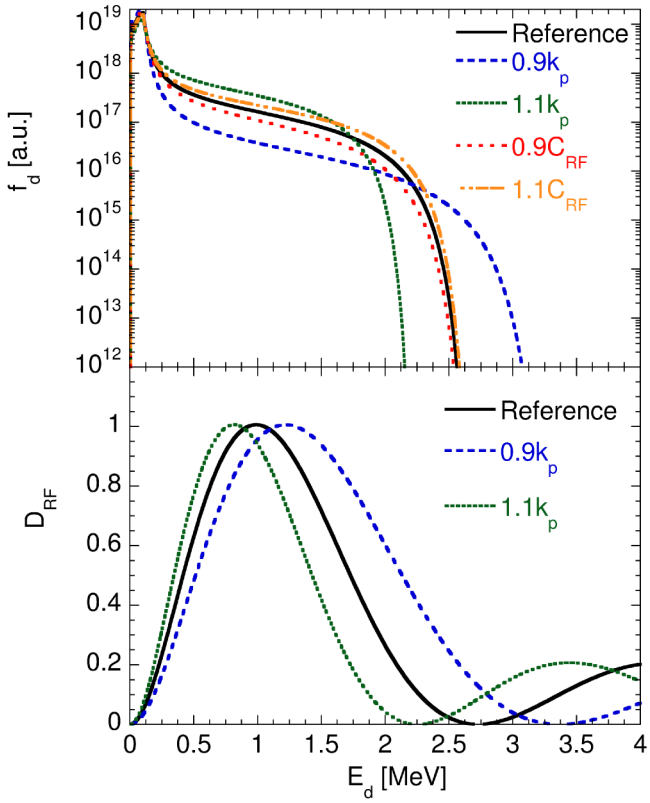

FIG. 2. (Top) Fast deuteron distribution function from 3rd harmonic heating obtained by solving Eq. (2) and setting $k_\perp = 47.5$ m^{-1} and $C_{\mathrm{RF}} = 9 \times 10^{13}$ m^2 s^{-3}. The corresponding quasilinear RF diffusion coefficient D_{RF} is shown in the bottom. The distributions obtained by varying $k_\perp$ and D_{RF} by ±10% around their mean values are represented by dashed and dotted lines in the top figure.

to be the best fit for one of the three discharges considered in this paper (see below). It is interesting to note that the fast ion distribution function generated by 3rd harmonic heating is highly non-Maxwellian and characterized by an extended but relatively flat tail in the phase space up to a certain cut-off energy, where a steep falloff of the distribution function occurs. This coincides with the appearance of the first zero of the D_{RF} coefficient (Figure 2 bottom), which has an oscillatory behavior conveyed by the Bessel functions in Eq. (3). The low energy part of the distribution ($E_d < 100$ keV) reflects the shape expected from NBI slowing down. The effect of changes in the $k_\perp$ and D_{RF} parameters on the distribution function is also investigated in Figure 2. The cut-off energy is varied by changes in $k_\perp$, which however also modify the intensity of the relatively flat tail. C_{RF} has no effect on the cutoff and describes only the RF power coupling efficiency, as a larger C_{RF} increases the flat tail level with respect to the $E_d < 100$ keV region due to beam ion slowing down.

IV. EXPERIMENTAL RESULTS

We here focus on the three JET discharges of the 3rd harmonic experiment (#86459, 86461, and 86464) which had the highest neutron yield (up to 6×10^{15} n/s). In all cases, the on-axis magnetic field was 2.25 T and the applied ICRH frequency was 51 MHz. In this configuration, the ion cyclotron resonance layer for deuterium heating at the 3rd harmonic was

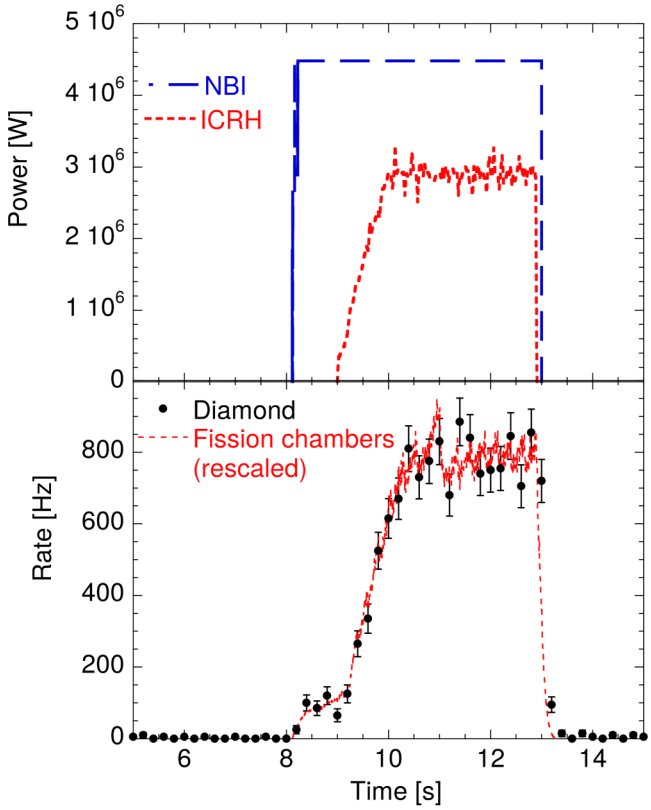

FIG. 3. (Top) Heating waveforms of NBI and ICRH applied in JET discharge #86459 (which had the highest neutron yield) and corresponding neutron counting rate measured by the SDD (bottom). The (rescaled) neutron counting rate measured by the JET fission chambers is also shown for comparison.

located close to the plasma center, at a major radius R = 3.1 m. The core electron density n_e was similar for 86459 and 86461 ($n_e \approx 4 \cdot 10^{19}$ m^3), for which 3 MW of ICRH and 4.5 MW of NBI were applied. A slightly higher core electron density ($n_e \approx 5 \cdot 10^{19}$ m^3) was found in discharge 86464, which was heated by means of 4 MW of ICRH and 2.5 MW of NBI. Figure 3 shows the time evolution of the heating pattern applied in discharge 86459 and the corresponding counting rate measured by the SDD. A factor 8 increase in neutron emission is found when ICRH is applied on top of NBI. Such

TABLE I. $k_\perp$ and C_{RF} parameters used to fit the SDD spectra of Figure 6 as derived from measurements with the TOFOR time of flight spectrometer at JET within the 1 dimensional generalized Stix model of Section III. The Cash-stat value obtained in each fit is also reported in the table, together with the number of degrees of freedom within parentheses. E* indicates the cut-off energy of the distribution function obtained in each discharge.

	86459	86461	86464
$k_\perp$ (m^{-1})	47.5	47.5	50.6
C_{RF} (m^2 s$^{-3}\times 10^{13}$)	9.0	11.0	15.0
E* (MeV)	2.72	2.72	2.40
C-stat	42.0 (33)	48.2 (33)	20.6 (33)

enhancement reflects the acceleration of beam ions to energies of a few MeVs, where the cross section for dd neutron emission is about an order of magnitude higher than that at typical JET beam energies (about 100 keV). This significant increase in neutron emission is a known feature of this heating scenario[5,8] and was observed in each of the three discharges considered in this analysis. Figure 4 shows the corresponding energy deposition spectrum measured by the SDD and integrated over the whole heating phase. For comparison, a sum of 45 similar spectra measured in JET NBI plasmas in 2013[27] and normalized to data for 86459 is also shown. In all cases, the high energy tail of SDD spectra from the 3rd harmonic experiment extends well beyond that observed in plasmas heated by NBI only and is interpreted as due to the acceleration of deuterons to the MeV range.

For a quantitative analysis of the SDD data, we made use of the one dimensional model for 3rd harmonic ICRH with input values for $k_\perp$ and C_{RF} as summarized in Table I. These were taken from results of an analysis based on data from the TOFOR time of flight spectrometer,[34,35] which was operational in the experiment and observes the plasma along a vertical line of sight. The corresponding deuteron distributions are shown in Figure 5. Discharges 86459 and 86461 had the same deuteron cut-off energy and a comparable intensity of the non-Maxwellian tail in the velocity space. 86464 had instead a E^* lower by about 300 keV.

The GENESIS code[32,33] was used to calculate the expected neutron spectrum resulting from deuterons described

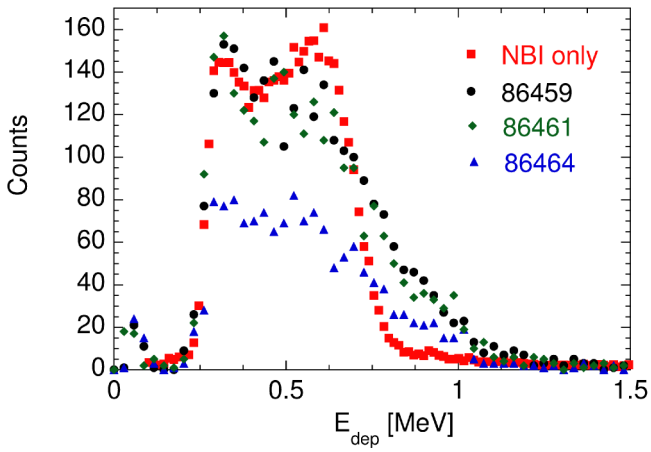

FIG. 4. Energy deposition spectrum measured for JET discharges 86459, 86461, and 86464 and compared to a sum of 45 similar spectra (normalized to same scale) measured at JET in 2013 in plasmas with NBI only.

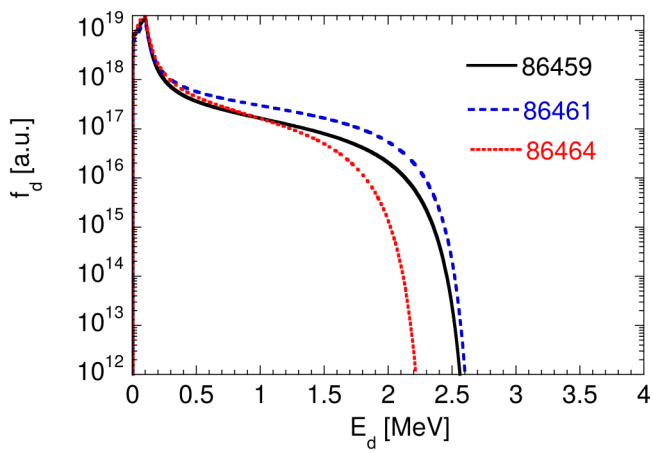

FIG. 5. Deuteron energy distributions derived from a fit of the TOFOR data of discharges 86459, 86461, and 86464 within the one dimensional model of Section III.

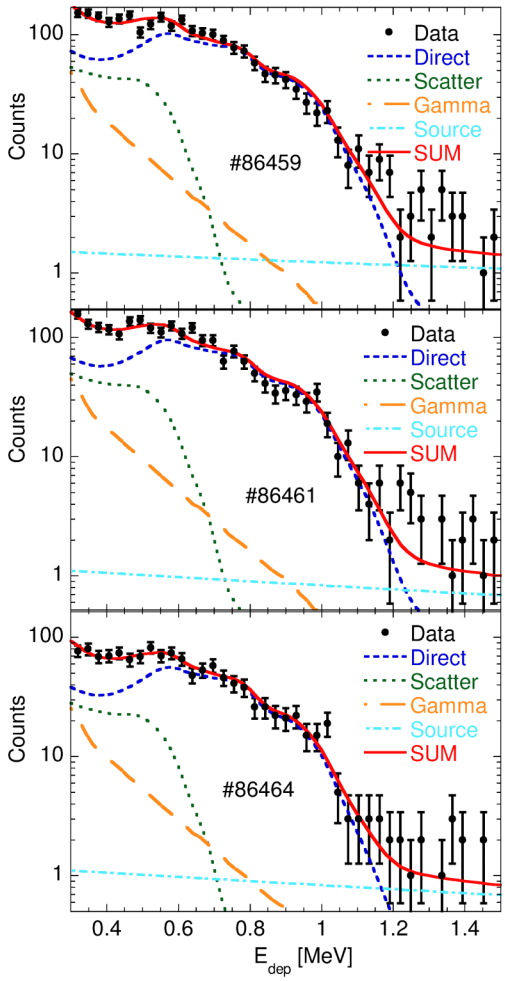

FIG. 6. Energy deposition spectrum measured in discharges 86459, 86461, and 86464 and fit to data. Components due to plasma neutrons impinging on the device (direct), scattered neutrons (scatter), and the associated background gamma-rays (gamma) are considered in the fit, besides the background from the triple-alpha calibration source (source). An additional high energy background due to neutrons from photo-dissociation (see text for details) is also included, but not shown as a separate fit component. The "direct" component was evaluated with GENESIS from each input deuteron distribution function as described in the text. The "scatter" and "gamma" components are the results of background calculations at the detector performed with MCNP. Each component has been convolved with the detector response function (evaluated with MCNP) before fitting.

by the 1 dimensional energy distributions of Figure 5 and reacting with a thermal plasma. In this calculation, neutron emission is assumed to be localized in the core plasma and evaluated for an angle of 47° with respect to the magnetic field to accommodate the detector line of sight. The neutron spectrum impinging on the detector (direct component) was finally folded with the instrument response function evaluated with MCNP (see Section II) for comparison with data. Figure 6 shows a fit to measured data for the three discharges. In each case, besides the direct component, energy down scattering of neutrons due to interactions with the MPRu housing as well as the associated background gamma-ray production was calculated with MCNP[27] and is indicated by the "scatter" and "gamma" dashed lines in the figure. A further background contribution ("source") is given by the known activity of the triple alpha calibration source, together with an additional flat background of less than 1 count/channel found at high deposited energies ($E_{dep} > 1.5$ MeV corresponding to $E_n > 5.3$ MeV) and which may be interpreted as due to additional neutrons from photo-dissociation. These high energy neutrons are also observed in the TOFOR data. Although four components are needed to describe the SDD data, only one fit parameter was used, i.e., the overall normalization to convert from the expected neutron/s in each energy bin of the spectrum to counts/channel measured by the SDD. The relative ratio between the intensities of the different components was kept fixed and evaluated with MCNP ("scatter" and "gamma" with respect to "direct") or by a fit to the background at high energies, out of the energy range of interest for this analysis ($E_{dep} < 1.5$ MeV). The Cash statistics[36] (C-stat) was used to evaluate the goodness of the fit, with values reported in Table I for each discharge. In all cases, a good fit to data was obtained.

V. DISCUSSION

Besides the SDD, two more instruments were used in this experiment to measure the neutron emission spectrum: TOFOR, looking vertically towards the plasma centre, and a NE213 liquid scintillator detector[26,37] installed behind the SDD in the MPRu dump and sharing its same oblique line of sight. Both instruments have a higher efficiency to dd neutron emission and were able to measure data at higher statistics. Figures 7 and 8 show the results of the fit to the TOFOR and NE213 data, respectively, for discharge 86459. As far as TOFOR is concerned, the neutron spectrum is measured in terms of the time of flight t_{TOF} of neutrons that scatter between two set of start-stop detectors of the instrument. $t_{TOF} = 65$ ns corresponds to $E_n = 2.5$ MeV. In the case of the NE213, instead, the neutron spectrum is measured as a histogram of the light emission from protons scattered by neutrons impinging on the device. Channel 45 corresponds to the maximum light emitted by a proton born from a 2.5 MeV neutron. For both instruments, a very good description of the data was obtained (reduced C-stat ≈1). From the fit to

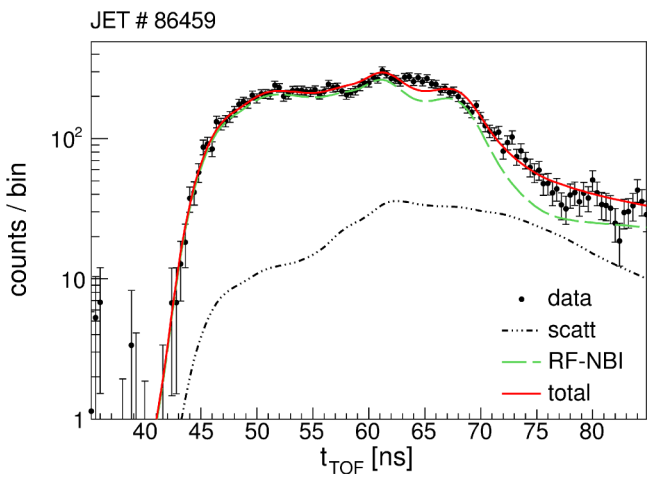

FIG. 7. Neutron spectrum measured by the TOFOR time of flight spectrometer in discharge 86459. A fit to the data using the model described in Section III is also shown (RF-NBI). The fit includes also a component from scattering of neutrons along their path from the plasma to the detector (scatter).

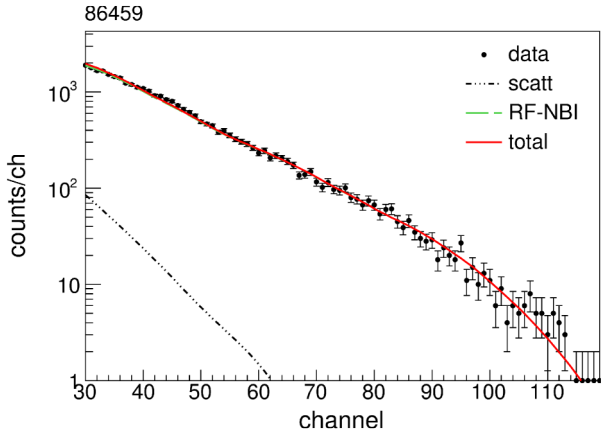

FIG. 8. Neutron spectrum measured by the NE213 liquid scintillator detector in discharge 86459. A fit to the data using the model described in Section III is also shown (RF-NBI). The fit includes also a component from scattering of neutrons along their path from the plasma to the detector (scatter).

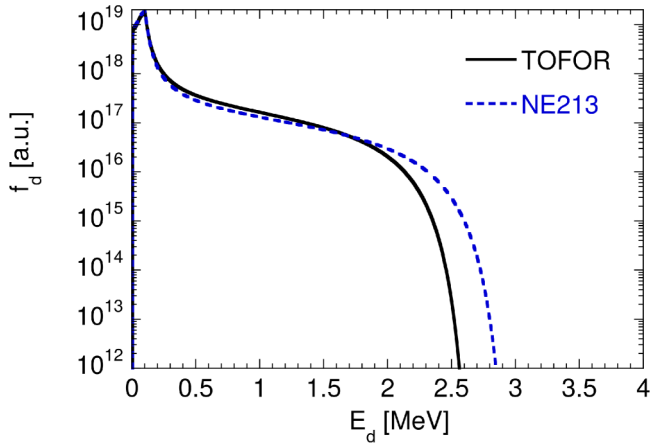

FIG. 9. Deuteron energy distribution derived from the fit to the TOFOR and NE213 data for discharge 86459 within the one dimensional model of Section III.

the data of each instrument, a set of $k_\perp$ and C_{RF} parameters was extracted (see Table II) and used to reconstruct the corresponding deuteron distribution function within the one dimensional model presented in Section III (see Figure 9).

Quite surprisingly, a different cut-off energy was found for the energy distributions derived with the two instruments, being $E^* = 2.7$ MeV for TOFOR and $E^* = 3$ MeV for the NE213. As fully discussed in references,[34,35] this difference is well above the uncertainty on the cut-off energy (about 1%). In the same reference, the discrepancy is explained by the different phase space sensitivity of neutron measurements along a vertical and oblique line of sight. In fact, neutron measurements along an oblique line of sight, as for the NE213 and unlike TOFOR, are sensitive especially to ions with pitch angles quite far from 90°,[38,39] which are not correctly described within the 1 dimensional model approximation of Section III, where $v \approx v_\perp$ is assumed instead. As countercheck, the authors of Refs. 34 and 35 demonstrate that parameters derived from the NE213 can be made to agree with those of TOFOR, within error bars, by artificially widening the pitch angle range of the fast ions to the 70°-110° interval.

Based on this evidence, we have further investigated the sensitivity of the fit to SDD data for 86459 within the 1 dimensional Stix model by letting $k_\perp$ and C_{RF} vary in the range 25-60 m^{-1} and $1 \cdot 10^{13}$–$3 \cdot 10^{14}$ m^{-2} s^{-3}, respectively, and evaluating the quality of each fit by means of C-stat. The aim of this sensitivity study was to determine whether the $k_\perp$ and C_{RF} parameters derived from an unconstrained fit of the SDD measurements and corresponding to the best fit for discharge 86459 were closer to those of the NE213 detector (same line of sight) rather than those of TOFOR (different line of sight). The resulting map as a function of $k_\perp$ and C_{RF} is shown in Figure 10. Calculations were performed both in the 1 dimensional model assumption that $v \approx v_\perp$ and by letting the pitch angle of the fast ions be distributed uniformly in the 70°-110° range. In order to facilitate the comparison with the NE213 and TOFOR analysis, we have restricted the fit to data in the time slice 10.5–12.1 s, where neutron emission is stationary, implying that the fast ion energy distribution has reached its steady state. From Figure 10, we find that contours at constant C-stat have shapes close to equilateral hyperbolas, suggesting a correlation between $k_\perp$ and C_{RF} as derived from fitting. C-stat increases significantly by changes of the parameters along the gradient perpendicular to the equilateral hyperbolas. This implies that, if either $k_\perp$ or C_{RF} were known, there would be only a very narrow interval of values for the other parameter where an acceptable fit to the SDD data is obtained. It is also interesting to note that the minimum C-stat occurs for a $k_\perp$ value that is lower than that derived from TOFOR (vertical line of sight), in agreement with the NE213 analysis[34,35] (same line of sight; see Table II). This is further supported by the regions associated to 68% and 90% confidence levels around the $k_\perp$ and C_{RF} values at the minimum C-stat (Min C) for the two pitch angle assumptions (1D model and 70°-110°) and can be used to investigate whether a signature of the predicted[38,39] phase space sensitivity of the oblique SDD line of sight to ions with pitch angles away from 90° can be traced in the SDD data. In the case of $v \approx v_\perp$ (1D model), a Cash-stat of 30.3 is obtained at the minimum and the surface corresponding to the 68% confidence level around C min includes the NE213 values that give the best fit to data,[34,35] but excludes TOFOR values, which can only be enclosed if we increase the confidence level to 90%. The situation is different in the large pitch angle case, where both TOFOR and NE213 values are comprised within the 68% confidence level around min C, in agreement with the pitch angle sensitivity study of Refs. 34 and 35. Both observations support the analysis of Refs. 34 and 35 and seem to confirm that the discrepancy between values inferred from the NE213 (and SDD at C min) and TOFOR is due to the different sensitivities to the phase space of the fast ions by measurements along vertical (TOFOR) and oblique (NE213 and SDD) lines

TABLE II. $k_\perp$ and C_{RF} values derived from the fit to the TOFOR and NE213 data for discharge 86459. The corresponding cut-off energies E^* of the deuteron energy distribution are also reported in the table.

	TOFOR	NE213
$k_\perp$ (m^{-1})	47.5	45.0
C_{RF} (m^2 $s^{-3} \times 10^{13}$)	9.0	10.0
E^* (MeV)	2.7	3.0

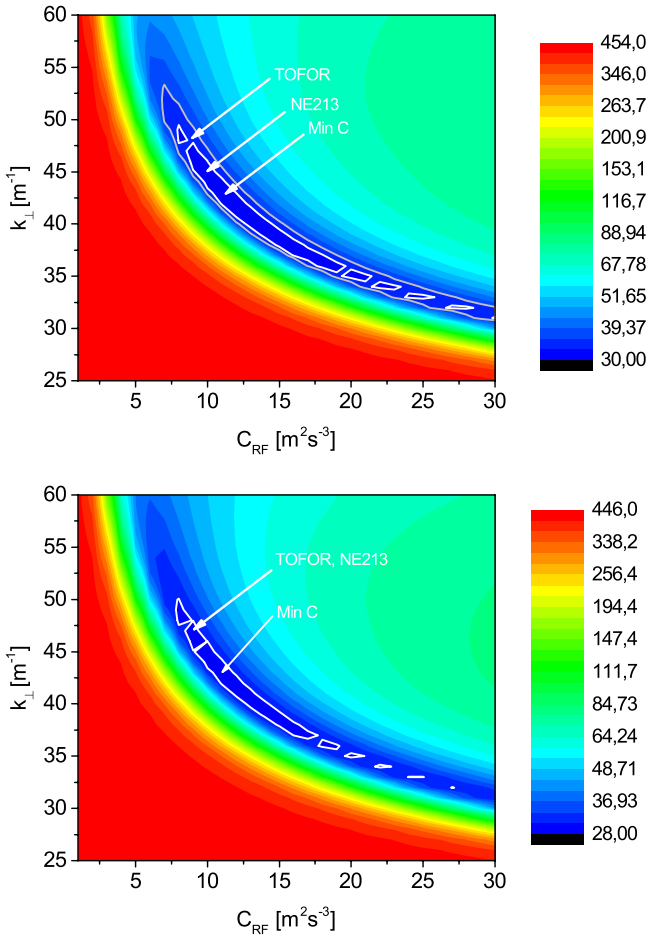

FIG. 10. Map of C-stat values obtained by fitting the SDD data for discharge 86459 in the time window 10.5-12.1 s and for different $k_\perp$ and C_{RF} values in the range 25-60 m^{-1} and $1 \cdot 10^{13}$–$3 \cdot 10^{14}$ m^2 s^{-3}, respectively. White arrows indicate C-stat values corresponding to fits with $k_\perp$, C_{RF} parameters derived from the analysis of TOFOR and the NE213 data in Refs. 34 and 35. White and grey lines bound regions associated to 68% and 90% confidence levels around $k_\perp$ and C_{RF} values at which a minimum C-stat (Min C) is found. Results are shown both in the 1 dimensional model assumption that $v \approx v_\perp$ (top) and by letting the pitch angle of the fast ions be distributed uniformly in the 70°-110° range (bottom).

of sight rather than to inconsistencies between separate detectors.

VI. CONCLUSIONS

Neutron spectroscopy measurements along an oblique line of sight with a SDD were performed in JET plasmas heated by ion cyclotron resonance heating at the third harmonic coupled into an injected beam of deuterons in a deuterium plasma. Neutrons with energies up to about 5.5 MeV were observed by the SDD and their spectrum successfully interpreted by means of the extended 1 dimensional Stix model for 3rd harmonic radio frequency heating. Parameters of the fast ion energy distribution, such as the perpendicular wave number $k_\perp$ that determines the high energy cut off and the radio frequency coupling coefficient C_{RF}, were derived from data. A detailed analysis of the fit sensitivity to changes in parameters of the fast ion distribution further revealed some limitations of the 1 dimensional Stix model to interpret measurements along an oblique line of sight and confirmed the conclusions inferred from neutron spectroscopy observations with other instruments in the same experiment. The results presented in this paper demonstrate the capability of SDDs to measure the fast ion energy distribution from 3rd harmonic radio frequency heating and are of relevance in view of the application of such detectors for spectroscopy measurements in the neutron camera of next step tokamak devices.

ACKNOWLEDGMENTS

This work has been carried out within the framework of the EUROfusion Consortium and has received funding from the Euratom research and training programme 2014-2018 under Grant Agreement No. 633053. The views and opinions expressed herein do not necessarily reflect those of the European Commission.

[1]W. A. Fisher *et al.*, Phys. Rev. A **28**, 3121 (1983).
[2]M. Nocente *et al.*, Nucl. Fusion **54**, 104010 (2014).
[3]C. Hellesen *et al.*, Plasma Phys. Controlled Fusion **52**, 085013 (2010).
[4]C. Hellesen *et al.*, Nucl. Fusion **55**, 023005 (2015).
[5]C. Hellesen *et al.*, Nucl. Fusion **53**, 113009 (2013).
[6]M. Gatu Johnson *et al.*, Nucl. Fusion **50**, 045005 (2010).
[7]M. Tardocchi *et al.*, Plasma Phys. Controlled Fusion **55**, 074014 (2013).
[8]C. Hellesen *et al.*, Nucl. Fusion **50**, 084006 (2010).
[9]T. Gassner *et al.*, Phys. Plasmas **19**, 032115 (2012).
[10]M. Gatu Johnson *et al.*, Nucl. Instrum. Methods Phys. Res., Sect. A **591**, 417 (2008).
[11]X. Zhang *et al.*, Nucl. Fusion **54**, 104008 (2014).
[12]X. Zhang *et al.*, Rev. Sci. Instrum. **85**, 043503 (2014).
[13]E. Andersson Sunden *et al.*, Nucl. Instrum. Methods Phys. Res., Sect. A **610**, 682–699 (2009).
[14]J. Källne *et al.*, Phys. Rev. Lett. **85**, 1246 (2000).
[15]M. Nocente *et al.*, Nucl. Fusion **51**, 063011 (2011).
[16]M. Nocente *et al.*, Nucl. Fusion **53**, 053010 (2013).
[17]M. Rebai *et al.*, J. Instrum. **7**, C05015 (2012).
[18]M. Rebai *et al.*, J. Instrum. **8**, P10007 (2013).
[19]C. Cazzaniga *et al.*, Rev. Sci. Instrum. **85**, 11E101 (2014).
[20]A. V. Krasilnikov *et al.*, Rev. Sci. Instrum. **68**, 553 (1997).
[21]A. V. Krasilnikov *et al.*, Nucl. Instrum. Methods Phys. Res., Sect. A **476**, 500 (2002).
[22]G. Knoll, *Radiation Detection and Measurements*, 4th ed. (Wiley, 2010).
[23]M. Mantsinen *et al.*, Phys. Rev. Lett. **88**, 105002 (2002).
[24]M. Nocente *et al.*, Nucl. Fusion **52**, 063009 (2012).
[25]J. Eriksson *et al.*, Plasma Phys. Controlled Fusion **55**, 015008 (2013).
[26]F. Binda *et al.*, Rev. Sci. Instrum. **85**, 11E123 (2014).
[27]C. Cazzaniga *et al.*, Rev. Sci. Instrum. **85**, 043506 (2014).
[28]See www.cividec.at for CIVIDEC.
[29]See https://mcnp.lanl.gov/ for MCNPX code website.
[30]T. H. Stix, *Waves in Plasmas* (Springer, New York, 1992).
[31]A. Salmi *et al.*, Plasma Phys. Controlled Fusion **48**, 717 (2006).
[32]M. Tardocchi *et al.*, Phys. Rev. Lett. **107**, 205002 (2011).
[33]M. Nocente, "Neutron and gamma ray emission spectroscopy as fast ion diagnostics in fusion plasmas," Ph.D. thesis, Università di Milano-Bicocca, 2012, http://boa.unimib.it/handle/10281/28397.
[34]J. Eriksson *et al.*, "Dual sightline measurements of MeV range deuterons with neutron and gamma-ray spectroscopy at JET," Nucl. Fusion (submitted); a draft version is available online at http://users.euro-fusion.org/repository/pinboard/EFDA-JET/journal/41893_ng-paper_03_8_2015.pdf.
[35]J. Eriksson, "Neutron emission spectrometry for fusion reactor diagnosis: Method development and data analysis," Ph.D. thesis, Uppsala University, 2015, http://uu.diva-portal.org/smash/get/diva2:798599/FULLTEXT01.pdf.
[36]W. Cash, Astrophys. J. **228**, 939 (1979).
[37]F. Binda *et al.*, "A practical approach to the analysis of neutron-induced NE213 pulse height spectra measured during third harmonic radio-frequency heating experiments at JET" (unpublished).
[38]A. S. Jacobsen *et al.*, Nucl. Fusion **55**, 053013 (2015).
[39]M. Salewski *et al.*, Nucl. Fusion **55**, 093029 (2015).